



Removal of phenolphthalein by aspartame functionalized dialdehyde starch nano-composite and optimization by Plackett–Burman design

Somayeh Heydari¹ · Leili Zare¹ · Saeedeh Eshagh Ahmadi¹

Received: 14 December 2020 / Accepted: 7 May 2021 / Published online: 27 May 2021
© Iranian Chemical Society 2021

Abstract

In this study, Plackett–Burman (P–B) experimental design combined with response surface methodology (RSM) of central composite design (CCD) was applied to study the removal of phenolphthalein (Php) from aqueous solution by aspartame functional magnetic dialdehyde starch nano-composite (APM-MDAS). This methodology enabled to identify the effects of the different factors studied and their interactions with a relative small number of experiments. By PBD, pH, sorbent dosage and contact time had a significant impact on Php removal. The maximum removal efficiency of phenolphthalein (95.41%) was achieved under the optimal conditions of pH, 10.68; sorbent dosage, 0.0015 (g mL⁻¹); contact time, 118.13 s. The experimental results were in good agreement with the predicted values, indicating that the integrated P–B and CCD design is an effective approach for the statistical optimization of Php removal process. The kinetics of Php sorption fitted well with pseudo-second-order kinetic model and the isotherm data of compound could be well described by Langmuir model. The results showed that with convenient magnetic operation and synthesized by common industrialized raw materials, the APM-MDAS nano-composite is a novel, easy to prepare, environmentally friendly and effective adsorbent for the removal of phenolphthalein from aqueous solution. Additionally, the P–B design followed by the CCD method is an effective and powerful approach for the optimization of sorption process.

Keywords Removal · Phenolphthalein · Aspartame functionalized nano-composites · Plackett–Burman design · Water treatment

Introduction

In the past few decades, the threat and risk of organic pollutants have become a major environmental concern due to the rapid industrial development in the world. These contaminants have posed significant risk to human and environment due to their carcinogenicity, mutagenicity and teratogenic properties in the biological system [1, 2]. Thus, there is an urgent need for the removal of organic pollutants using an effective, efficient and affordable method.

Several methods such as physicochemical [3], chemical [4], biological [5], electrochemical [6] and advanced oxidation processes (AOPs) approaches [7] were used to remove organic pollutants from wastewater. Adsorption is one of the promising techniques for the removal with regard to ease

of operation, cost economics, greater flexibility, easy availability, insensitivity to toxic substances and its effectiveness even in dilute solutions [8]. Various adsorbent materials have been used to remove the organic compounds from aqueous media [9]. Among these adsorbents, natural polymers, mainly polysaccharides such as starch, chitosan and its derivatives and synthetic polymers, including polyaniline, polypyrrole and polyacrylonitrile, were found to be highly efficient adsorbents [10, 11]. However, some disadvantages like toxic monomer, crosslinking agent, low surface area and difficult separation procedures from the aqueous phase still are inevitable in the use of synthetic polymer composite and natural polymer composite, respectively. Accordingly, synthesis of the environmental friendly novel adsorbents and their modified derivatives to improve the adsorption with a simple way is yet an arduous task.

Starch is a green renewable biopolymer owing to its wide availability, non-toxicity and low cost. Modified starch for the applications in various areas can be obtained by physical, chemical and enzymatic methods. Dialdehyde starch

✉ Somayeh Heydari
so_heydari_83@yahoo.com

¹ Department of Chemistry, University of Torbat-e jam, Torbat-e jam, Iran

(DAS) is one kind of modified starch that contains many active aldehyde groups and widely used as a cross-linking agent [12].

Currently, magnetic Fe_3O_4 materials have attracted much interest in many environmental engineering-related applications due to their easy preparation, low toxicity, abundant active sites, excellent sorption capacities and effective magnetic separation [13–17]. To protect the magnetic Fe_3O_4 and provide a better surface specificity to remove of different contaminants, many researches have been focused on modification of the magnetic material [18].

In recent years, magnetic organic–inorganic nano-composites have been studied for the development of new advanced functional materials and shown remarkable potential in the field of removal because their abundant functional groups on the surface and high adsorption capacity. In this work, we first fabricated magnetic dialdehyde starch nano-composite (MDAS) using Fe_3O_4 as the core layer and DAS as shell layer through covalently linking the dialdehyde starch and amine functionalized Fe_3O_4 nanoparticle via Schiff base. After further modified with aspartame, the as-prepared nano-composite was used for the uptake of organic pollutant, phenolphthalein (Php) from contaminated wastewater. In this work, DAS was used to stabilize the Fe_3O_4 nanoparticles and inhibit their aggregation, while the aspartame was applied to functionalize the nano-composites so as to obtain selective phenolphthalein removal from contaminated water. The composition and structure of the resulting adsorbent were studied with the help of characterization methods. The performance of the nano-composite in the removal of Php was estimated using UV–Vis spectrophotometry and the effect of operational parameters was evaluated using Plackett–Burman design. The conventional method of studying a process is by varying one factor at a time while others are fixed. This is not only time consuming, but also inadequate to evaluate the interactions between variables or factors. The mentioned limitations of classical methods can be overcome by introducing statistically experiment design [19]. The Plackett–Burman (P–B) design, first described in 1946, is usually used to identify the most important factors among a large number of variables that could influence a studied phenomenon [20]. The main advantage of this experimental design is to deliver as much information as possible with a relative small number of experiments. After determining the influencing variables, it is necessary to further optimize the values of these parameters. Here, the impact of various factors was investigated by the response surface methodology of CCD. In addition, we also studied the kinetics of sorption and isotherms to analyze the adsorption mechanism and investigate the interaction between aspartame functional magnetic dialdehyde starch nano-composite (APM-MDAS) and Php. All in all, the goal is to develop a novel magnetic adsorbent with low-cost,

green raw materials, facile synthetic processes and large adsorption capacity to remove organic compound, Php from contaminated wastewater and optimize adsorption process variables by P–B design, and CCD method.

Experimental section

Materials

Potato starch (food-grade) was procured from grocery. It was dried at 105 °C before usage. Chemicals and reagents sodium periodate, $\text{FeCl}_3 \cdot 6\text{H}_2\text{O}$, 2-aminoethanol, anhydrous sodium acetate, ethylene glycol and aspartame were obtained from Merck. Php analytical grade was purchased from Merck and used without further purification. Stock solution (1000 mg L^{-1}) of Php was prepared by direct dissolution of proper amounts of Php in methanol and diluted with deionized water to obtain working standard solution. The solution pH was adjusted by mixing with proper volumes of 0.01 M NaOH solution. Freshly prepared double distilled deionized water was used throughout the experiment.

Preparation of $\text{NH}_2\text{-Fe}_3\text{O}_4$ nanoparticles

The first synthesis step is the preparation of amine-functionalized magnetite Fe_3O_4 nanoparticles ($\text{NH}_2\text{-Fe}_3\text{O}_4$) according to the previous reported method [21]. Typically, 1.0 g of anhydrous FeCl_3 and 2.0 g of anhydrous sodium acetate were added to 30 mL of ethylene glycol, and subsequently 10 mL of 2-aminoethanol was added to obtain a limpid solution via reflux. This mixture was then transferred into a Teflon-lined autoclave and heated at 200 °C for 8 h [22]. $\text{NH}_2\text{-Fe}_3\text{O}_4$ was separated from the solution by the external magnet and washed with deionized water thoroughly. Finally, magnetite nanoparticles were dried at 60 °C of 24 h under vacuum.

Preparation of DAS

The second step involves synthesis of dialdehyde starch (DAS) according to previous articles [21]. In a typical process, sodium periodate solutions (5.28 g) as an oxidant, was added to a mixture of potato starch (4.0 g in 10 mL of water) and adjusted pH to 3.5. The mixture was stirred in the dark condition at 30 °C for 4 h and filtered. DAS was washed with deionized water and ethanol for several times. The filtered solid was dried at 50 °C for 24 h under vacuum.

For the synthesis of magnetic dialdehyde starch nano-composite (MDAS), 0.25 g of DAS was added to 30 mL of the above magnetic nanoparticle suspension (contained 0.25 g $\text{NH}_2\text{-Fe}_3\text{O}_4$) and sonicated for 30 min with N_2

protection. The reaction temperature was risen to 90 °C for 2 h to obtain the MDAS.

Preparation of APM-MDAS nano-composites

In this step, magnetic dialdehyde starch nano-composite (MDAS) was prepared through covalently linking the dialdehyde starch and amine functionalized Fe₃O₄ nanoparticle by Schiff base. DAS (0.25 g) and NH₂-Fe₃O₄ nanoparticles (0.25 g) were added to 30 ml of deionized water, and then, the suspension was sonicated for 30 min with N₂ gas protection. After sonication, the reaction temperature was risen to 90 °C for 2 h to obtain the MDAS nano-composite. In the following, MDAS was modified with aspartame functional group. Typically, 0.28 g of aspartame (APM) in 15 mL deionized water was added to the system and kept in 60 °C for 2 h. The resulting product, APM-MDAS, was rinsed with deionized water and ethanol completely and dried in a vacuum oven at 60 °C for 24 h. Scheme for the synthesis route of APM-MDAS nano-composite was shown in Fig. 1.

Characterization of NH₂-Fe₃O₄ and APM-MDAS

Fourier transformed infrared (FTIR) spectroscopic study was done through FTIR (PerkinElmer 1750 FTIR) spectrophotometer within the range of 400–4000 cm⁻¹ to investigate the nature of formed chemical bond. The surface morphology of pure and functionalized magnetic nanoparticles was studied using field emission scanning electron microscope (SEM, TESCAN Mira3) operated at an accelerating voltage of 15 kV. The X-ray diffraction (XRD) studies were performed with a Philips XRD instrument

(Siemens D-5000, Germany) using Cu Kα radiation ($\lambda = 1.541874 \text{ \AA}$) in the range of 20–80° (2θ) at 40 kV of accelerating voltage and at 30 mA of emission current to determine the crystalline shape of magnetic nanoparticles.

Adsorption Experiments

Performance of APM-MDAS was investigated by the removal of Php in a batch system. Typically, 0.0015 g of APM-MDAS was dispersed in 10 mL of Php solution with initial concentration of 100 mg L⁻¹ adjusted to a desired pH value of 11.0 by adding dilute solutions of NaOH. At regular time intervals, 5 mL of aliquots were drawn and subsequently the adsorbent particles were separated rapidly by a magnet. The concentration of the Php solutions was determined at $\lambda_{\text{max}} = 565 \text{ nm}$ by a UV-Vis double-beam spectrophotometer (Photonix Ar 2017, UV-Vis Array). The equilibrium adsorption capacity (q_e) (mg g⁻¹) and removal efficiency (R) of Php were calculated by the following equations:

$$q_e = \frac{(C_o - C_e)V}{W} \quad (1)$$

$$R(\%) = \frac{(C_o - C_e)}{C_o} \times 100\% \quad (2)$$

where C_o and C_e were the compound concentrations before and after adsorption (mg L⁻¹), V is the volume of adsorbate (L) and w is the weight of adsorbent (g).

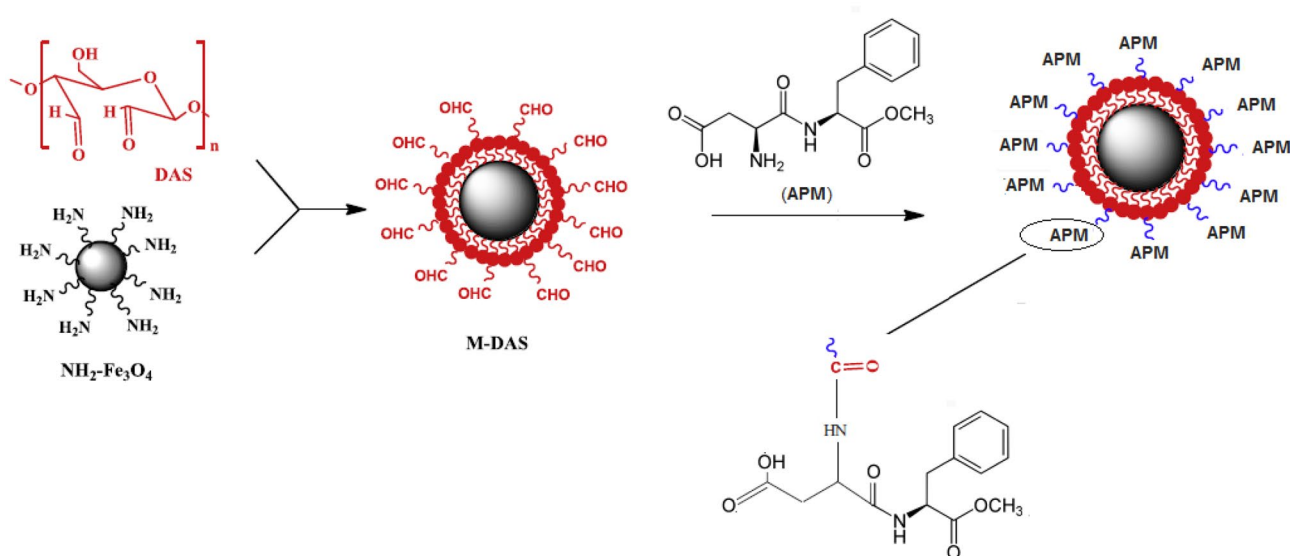


Fig. 1 Scheme for the synthesis route of APM-MDAS nano-composite

Table 1 Factors, codes, levels in the Plackett–Burman design matrix

Variable code	Variable	Low level (–)	High level (+)
A	pH	8	11
B	Amount of sorbent (g/ml)	0.001	0.003
C	Contact time (min)	90	120
D	Agitation speed	400	800

Table 2 Plackett–Burman design of variables in coded levels with Php removal efficiency as response

Run	A	B	C	D	Y (%)
1	10	0.001	120	400	63.72
2	10	0.003	90	800	43.00
3	8	0.003	120	400	27.00
4	10	0.001	120	800	55.85
5	10	0.003	90	800	41.00
6	10	0.003	120	400	56.34
7	8	0.003	120	800	20.21
8	8	0.001	120	800	32.00
9	8	0.001	90	800	35.00
10	10	0.001	90	400	72.50
11	8	0.003	90	400	30.00
12	8	0.001	90	400	40.00

Statistical analyses

In order to optimize the parameters affecting the proposed removal procedure, the effects of the main parameters were investigated using chemometric approach based on the Plackett–Burman (P–B) screening design and the central composite design (CCD).

In this study, a total of 12 runs P–B design were applied to evaluate the significance of four variables influencing removal, including pH, amount of sorbent, contact time and agitation speed. Each variable was tested at two levels (low and high). The level of each factor and its symbol is illustrated in Table 1. Before PBD experiments, the minimum and maximum of level for each factor were chosen according to the preliminary experiments. The P–B design was arranged by Minitab 17 (Minitab Inc USA) statistical software program, and the response values of Phenolphthalein removal efficiency (Y) are shown in Table 2. The main parameters were evaluated using

Table 3 Experimental range and levels of the significant variables in CCD

Variable	Low level (–)	Center level (0)	High level (+)
pH	8	9.5	11
Amount of sorbent (g mL ⁻¹)	0.0001	0.0012	0.0025
Contact time (min)	105	120	130

Pareto chart (Fig. 5). By plotting all the results of experiments on a Pareto chart, it would be easy to detect and compare the fundamental effects of all components.

In order to optimize the factors selected from the first screening P–B design, a central composite design (CCD) including 20 runs was developed. The levels of each factor and matrix of C–C design are shown in Tables 3 and 4, respectively. The data obtained from CCD method were fitted using the following second-order polynomial Eq. 3:

$$Y = b_0 + \sum_{i=1}^n b_i X_i + \sum_{i=1}^{n-1} \sum_{j=2}^n b_{ij} X_i X_j + \sum_{i=1}^n b_{ii} X_i^2 \quad (3)$$

where Y is the response variable to be modelled, X_i and X_j define the independent variables. n is the number of variables. b₀, b_i, b_{ii}, and b_{ij} are the constant coefficient, the linear coefficient, the quadratic coefficient and the interaction coefficient, respectively.

The adequacy of each model was checked using the F-values, lack of fit and R²-values, and finally a quadratic model was adopted. The statistical significance of the full quadratic models predicted was considered by the analysis of variance (ANOVA). The ANOVA results of the quadratic model are summarized in Table 5.

Results and discussion

Characterization of APM-MDAS nano-composite

SEM characterization

The morphologies of NH₂–Fe₃O₄ and APM-MDAS nano-composite were analyzed using the SEM images. As shown in Fig. 2, the NH₂–Fe₃O₄ nanoparticles (Fig. 2a and c) were spherical, and the uniform particle size was about 35.1 nm. The SEM images of APM-MDAS nano-composite (Fig. 2b and d) demonstrated that the morphology of nano-composites retained the same substantial as the NH₂–Fe₃O₄ nanoparticles. Therefore, the adsorption ability of the nano-composite has been demonstrated due to the excellent monodispersity and uniform morphology.

FTIR characterization

In order to study the nature of formed chemical bond in APM-MDAS nano-composites, the FTIR spectra of the pure NH₂–Fe₃O₄ nanoparticles and APM-MDAS nano-composite

Table 4 Experimental design and results of CCD

Run	pH	Amount of sorbent (g mL ⁻¹)	Contact time (min)	Y (%)	
				Actual	Predicted
1	10	0.0012	120	83.53	86.59
2	10	0.0010	120	84.89	84.69
3	11	0.0010	110	80.41	89.09
4	10	0.0012	120	81.51	86.59
5	11	0.0010	130	77.68	87.33
6	9	0.0020	130	51.01	55.59
7	11	0.0020	110	90.11	88.19
8	11	0.0010	120	95.13	95.69
9	8	0.0012	120	52.89	50.74
10	10	0.0012	120	70.50	86.59
11	9	0.0001	110	36.04	34.33
12	9	0.0020	110	49.99	51.16
13	10	0.0012	120	80.22	86.59
14	9	0.0010	120	62.01	69.53
15	9.5	0.0012	120	79.04	79.19
16	10	0.0025	120	63.11	62.98
17	11	0.0020	120	85.11	93.85
18	10	0.0012	105	64.12	63.33
19	10	0.0012	120	81.10	86.59
20	10	0.0012	120	82.21	86.59

were examined and shown in Fig. 3. As confirmed in the literature, peak in NH₂-Fe₃O₄ spectra (a) at 588.2 cm⁻¹ are related to the vibration of Fe–O functional group [23, 24]. Peak at 1614.7 cm⁻¹ indicates that the particle contains amount of amine group [25]. In APM-MDAS spectra (b), the

band of amine group in 1614 cm⁻¹ increased and the new band of aspartame group in 2332.6 cm⁻¹ formed. The peak at 2332.6 cm⁻¹ is ascribed to the NH stretching of the amino group involved in hydrogen bonding with the carboxylate residue. The peak at 3404.9 cm⁻¹ is corresponding to N–H stretching vibration overlaps with OH stretching, whereas the frequency at 2900.1 cm⁻¹ could be assigned to C–H stretching vibration. The symmetric frequency of COO⁻ observed at 1390.2 cm⁻¹ could be assigned to carboxylate stretching of aspartame on nano-composite. The low intensity peak at 930.4 cm⁻¹ is ascribed to the OH torsional and C–O stretching of carboxylate. A characteristic band between 500 and 650 cm⁻¹ can be associated with the stretching and torsional vibration modes of Fe₃O₄. These observations indicate that the nano-composite has been successfully synthesized.

XRD characterization

Figure 4 indicates the XRD pattern of APM-MDAS nano-composite. In the XRD pattern of nano-composite, the six characteristic diffraction peaks at 2θ = 30.1°, 35.5°, 43.3°, 53.4°, 57.2° and 62.5° marked by their indices (220), (311), (400), (422), (511) and (440). These peaks match well with pure magnetite reflections (JCPDS card no. 75-1610), which is a crystalline magnetite with a cubic inverse spinel structure. Moreover, the XRD patterns of APM-MDAS nano-composite were sharp and distinct without containing any other impure peaks, revealing that functional DAS has successfully introduced to the surface of the NH₂-Fe₃O₄ nanoparticle. The crystallite size APM-MDAS nano-composite

Table 5 ANOVA results of the polynomial model for Pnp removal

Source	Sum of squares	Degree of freedom	Mean square	F-Value	P-Value	
Model	5003.95	9	555.99	22.86	0.0002	Significant
A-pH	2620.89	1	2620.89	107.77	0.0001	
B- Amount of sorbent	124.44	1	124.44	5.12	0.0470	
C- Contact time	120.71	1	120.71	4.91	0.0490	
A ²	62.49	1	62.49	2.57	0.1400	
B ²	1549.12	1	1549.12	63.70	0.0001	
C ²	805.80	1	805.80	33.13	0.0001	
AB	52.58	1	52.58	2.16	0.1720	
AC	32.68	1	32.68	1.34	0.2730	
BC	3.93	1	3.93	0.16	0.6960	
Lack of fit	227.45	5	45.49	14.44	0.0050	Not significant
Pure error	15.75	5	3.15			
Core total	5247.14	19				
R-Squared			0.95370			
Adj R-Squared			0.91190			
C.V.%			1.26			
Adequacy precision			28.40			

Fig. 2 SEM image of $\text{NH}_2\text{-Fe}_3\text{O}_4$ (a) and (c); APM- MDAS (b) and (d)

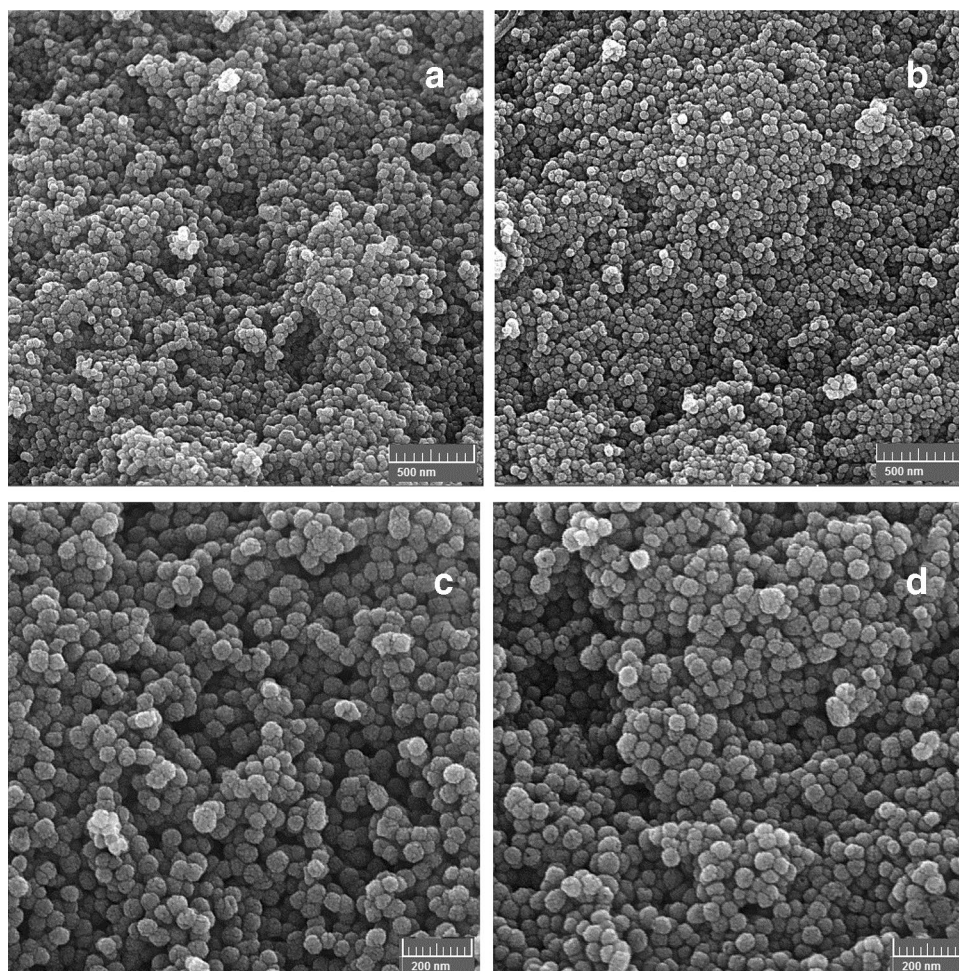


Fig. 3 FTIR spectrum of $\text{NH}_2\text{-Fe}_3\text{O}_4$ (a) and APM- MDAS (b)

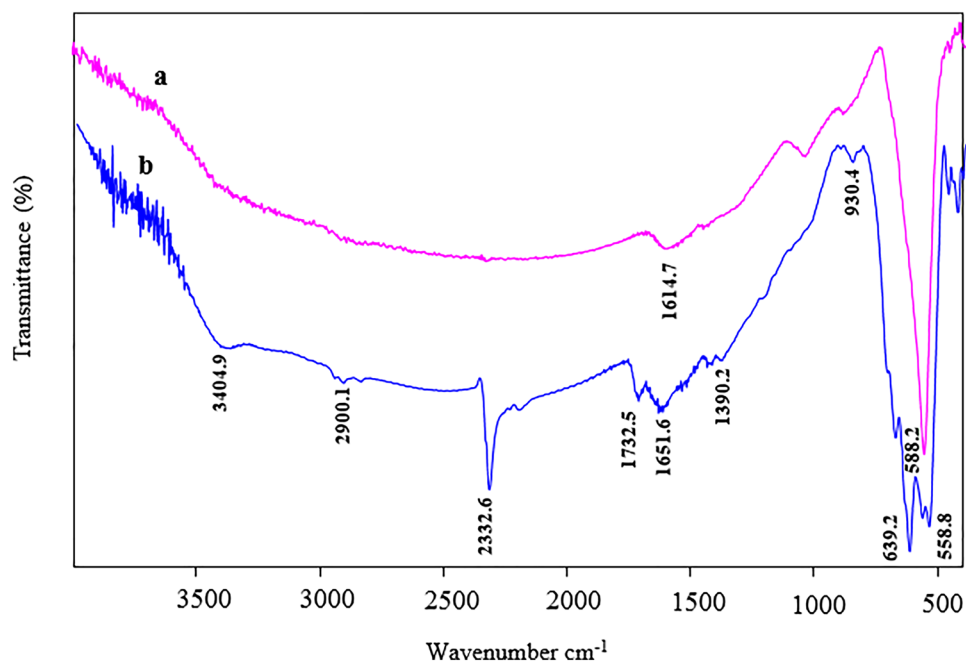
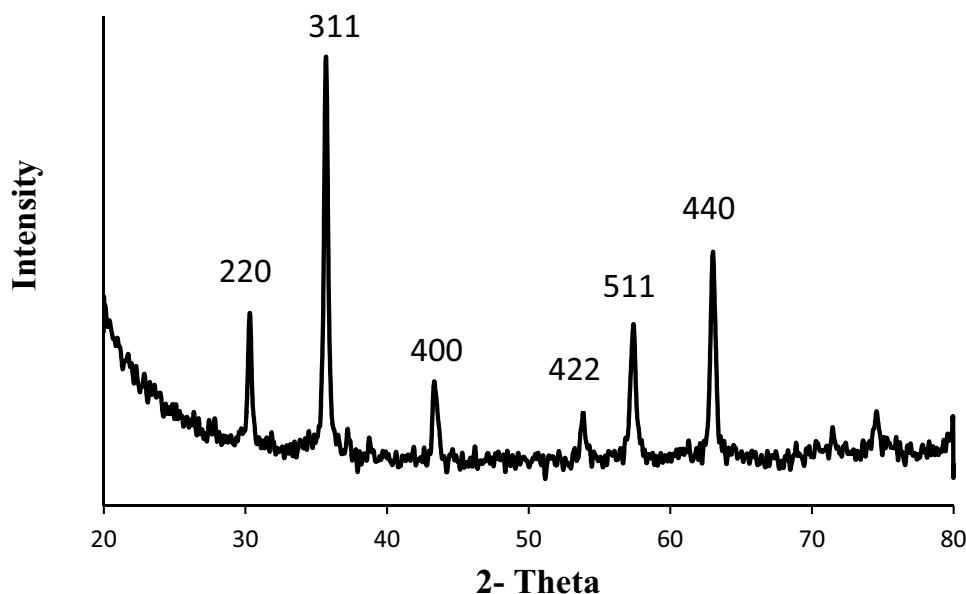


Fig. 4 XRD patterns of APM-MDAS nano-composite

was determined from its XRD pattern using the Scherrer equation [26]:

$$D = \frac{k\lambda}{\beta \cos \theta} \quad (4)$$

where D is the crystallite size of nanoparticles (nm), k is the Scherrer constant (the common value of 0.9, depending on the crystallite shape), λ is the X-ray wavelength (0.1541874 nm), β is the full width at half maximum (FWHM) and θ is the half of diffraction angle. We applied this equation to the best fitting highest intensity (311) XRD peak and estimated the crystallite size of APM-MDAS nano-composite to be about 32.6 nm. This result is in agreement with the average particle size of the nanoparticles obtained from the SEM image of the nano-composite.

Screening of significant variables using Plackett–Burman design

Plackett–Burman design was used to screen the relative importance of each factor (P_i) on the percentage removal of Php [27]. The analysis of results in Table 2 produced the standardized main effect Pareto chart using the following equation. The obtained results are shown in Fig. 5.

$$P_i = \left(\frac{b_i^2}{\sum b_i^2} \right) \times 100 \quad (i \neq 0) \quad (5)$$

The bar length is proportional to the significance of the variables for removal of compound. As such, pH, sorbent dosage and contact time appeared to be the significant

variables in affecting the uptake of Php. Agitation speed which had low importance affecting on removal was selected to be 600 rpm. Comparison between the three significant factors shows that pH is much more effective than the other two factors, but the effects of the other two factors on the removal of Php are much closer.

Optimization of significant variables using CCD

After the initial pH, sorbent dosage and contact time being determined to be the significant variables based on the P–B design, the optimum levels of these variables were further optimized by CCD. The experimental design, the corresponding results of CCD and the predicted values are shown in Table 4. By applying multiple regression analysis to the experimental data, the following second-order polynomial equation was found to explain the removal efficiency of Php:

$$\begin{aligned} C8 = & -1596 + 75.5A + 27141B + 20.18D - 2.08A \times A \\ & - 18431827B \times B - 0.0748D \times D \\ & + 3418A \times B - 0.202A \times D - 94B \times D \end{aligned} \quad (6)$$

The results listed in Table 5 indicated that the model was significant at 95% confidence interval (only 5% of the data cannot be processed by the suggested model) and adequate for reasonable prediction of the removal of compound within the variable range employed, as evidenced by the F -value (22.86) and the Prob > F value (0.0002). For each variable under studied, it is considered to be significant if it is having a value of Prob > F less than 0.05. It can be concluded from Table 5 that three main variables, i.e., pH, sorbent dosage and contact time, and quadratic terms of sorbent dosage and contact time, are clearly significant, while the interaction

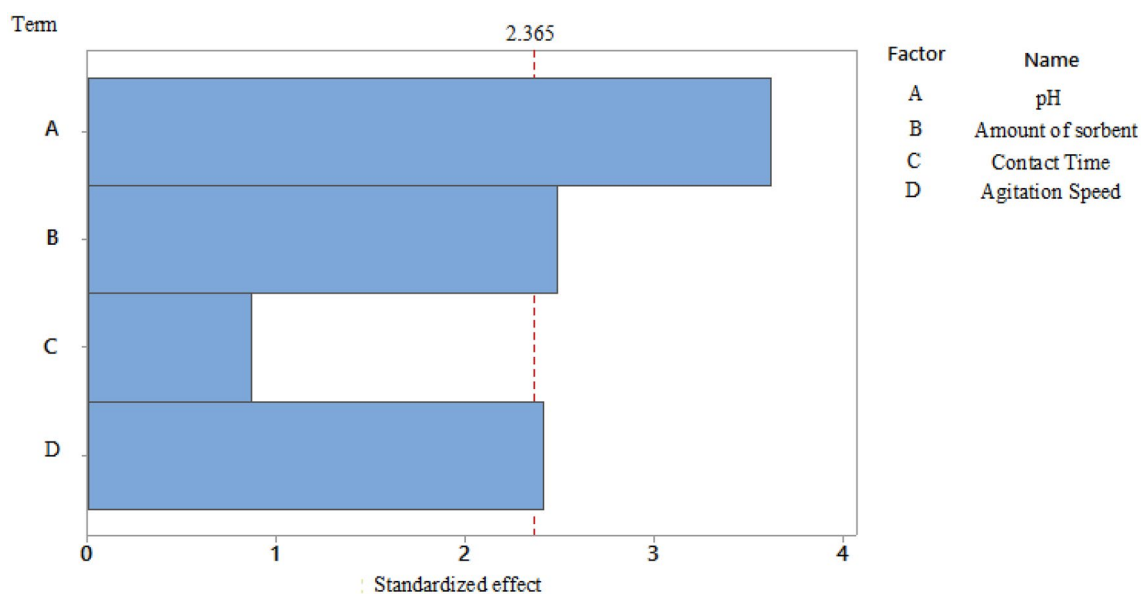


Fig. 5 Standardized main effect Pareto chart for Plackett–Burman design

between them is statistically insignificant. Also, according to the greater F-value (107.77), the initial pH is the most important variable of the response. It is well known that the pH of the Php solution influences the surface charge of the sorbent, the dissociation of functional groups presents on the sorbent as well as the degree of ionization of the Php. The lack of fit observed for model was 0.0050, with high values for R^2 (0.9537) and adjusted R^2 (0.9119). The results suggested that the “Lack of fit” was nonsignificant relative to the pure error. The closer the R^2 value of unity and the smaller the standard deviation implying more accurate response and repeatability that could be predicted by the model [28, 29]. The large adjusted R^2 value indicated the correspondence between the experimental data and the fitted model. The values of R^2 and adjusted R^2 indicated that the response equation provided a suitable model for the removal of Php. In general, a low coefficient of variation (CV) indicates that statistical model is effective and reliable [30]. In this case, CV for removal of Php was 1.26 that can be considered as another evidence for validity of the model. In addition, adequate precision value of 28.40, greater than 4, indicated good precision and reliability of the experiments.

After obtaining the fitted model for Php removal, the optimal values for significant factors were chosen: pH, 10.68; sorbent dosage, 0.0015 (g mL^{-1}); contact time, 118.13 s. The validity of the model was evaluated by the removal of Php for three replicate verification experiments under the optimum conditions and summarized in Table 6. The average of obtained experimental value was 95.41%, which agreed well with the predicted value. These results demonstrated that the statistical model is effective and reliable.

Adsorption kinetics and isotherm study

In order to evaluate the mechanism of adsorption process, Langmuir, Freundlich, Dubinin–Radushkevich (D–R) and Temkin isotherms are applied [31]. The linear equation of the Langmuir isotherm is expressed as follows:

$$C_e/q_e = 1/bq_m + C_e/q_m \quad (7)$$

where C_e is the equilibrium concentration of compound in solution (mg L^{-1}), and q_e is the equilibrium adsorption capacity (mg g^{-1}), q_m (mg g^{-1}) and b (L mg^{-1}) are the Langmuir constant which are related to the maximal monolayer adsorption extent of the adsorbent and energy of adsorption, respectively.

The linear expression of the Freundlich isotherm is shown below:

$$q_e = K_f C_e^{1/n} \quad (8)$$

where K_f is the Freundlich constant related to adsorption capacity. n represents the constant related to adsorption intensity. If n is greater than 1, the adsorption process is

Table 6 Predicted and experimental values of response at optimum conditions

pH	Adsorbent dose (g mL^{-1})	Contact time (min)	Response		Error
			Predicted (%)	Experimental (%)	
10.68	0.0015	118.13	95.63	95.41	0.23

favorable. Freundlich model directs toward heterogeneous adsorption indicating a multilayer sorption.

Dubinin–Radushkevich model is generally used to express the nature of adsorption as physically and chemical and can be presented as Eq. 9.

$$\ln q_e = \ln q_m - K_D \varepsilon^2 \quad (9)$$

where K_D is a constant related to the adsorption energy, and ε is the Polanyi potential which is equal to

$$\varepsilon = RT \ln (1 + 1/C_e) \quad (10)$$

In Dubinin–Radushkevich isotherm, the mean free energy, E (kJ mol^{-1}), shows the mechanism which sorption takes place and defined by Eq. 11

$$E = (2K_D)^{-1/2} \quad (11)$$

Value of mean free energy below 8 kJ mol^{-1} displays physical biosorption while a value between 8 and 16 kJ mol^{-1} indicates chemical biosorption.

The linear expression of the Temkin isotherm is as follows:

$$q_e = B \ln K_T + B \ln C_e \quad (12)$$

where B is RT/b , B is the variation of adsorption energy (J mol^{-1}) and K_T (L mg^{-1}) is the equilibrium binding constant.

The isothermal studies were carried out at various Php initial concentrations at pH 10.68. The range of Php initial concentration were $40\text{--}400 \text{ mg L}^{-1}$. After continuously stirring for 120 min, the adsorbent was collected by magnetic separation. The adsorption capacity of the adsorbent was measured by the difference between the initial and remaining concentration of Php. The details of the isotherm models are given in Table 7. The higher value of correlation coefficient ($R^2 = 0.9145$) revealed that the Php adsorption over the nano-composite well fitted better by the Langmuir model than by the Freundlich, D-R and Temkin model. Various parameters like q_m and b were calculated to be $833.333 \text{ mg g}^{-1}$ and 0.0248 L mg^{-1} . The results depicted a monolayer adsorption on the surface of adsorbent.

In APM-MDAS nano-composite, π - π interaction between benzene ring in the adsorbent and benzene ring of Php may also present. Additionally, the presence of amino group on the adsorption surface promotes the formation of hydrogen bonding with Php. The presence of hydrogen bonding and π - π interaction in APM-MDAS nano-composite results in a high adsorption capacity.

According to Dubinin–Radushkevich model, the mean free energy for adsorption of Php by the nano-composite is found to be $1.857 \text{ kJ mol}^{-1}$. This presents that predominant mechanism of the adsorption of Php by the nano-composite is likely physical sorption.

Table 7 Parameters of isotherm models on adsorption of Php using APM-MDAS nano-composite

Isotherm	Parameters					
Langmuir	q_m (mg g^{-1})	833.333	B (L mg^{-1})	0.025	R^2	0.914
Freundlich	K_f (mg g^{-1})	94.631	n (L g^{-1})	2.865	R^2	0.818
Dubinin–Radushkevich	K_D ($\text{mol}^2 \text{kJ}^{-2}$)	0.145	E (kJ mol^{-1})	1.857	R^2	0.899
Temkin	K_T (L g^{-1})	0.592	B (kJ mol^{-1})	85.661	R^2	0.851

Adsorption kinetics investigation provides an idea for understanding the adsorption mechanism. Adsorption kinetics based on pseudo-first-order and pseudo-second-order kinetic models were employed to interpret the experimental data and respectively represented as Eqs. (13) and (14):

$$\log (q_e - q_t) = \log q_e - k_1 t / 2.303 \quad (13)$$

$$t/q_t = 1/k_2 q_e^2 + t/q_e \quad (14)$$

where k_1 and k_2 are pseudo-first-order rate constant (min^{-1}), and pseudo-second-order rate constant ($\text{g mg}^{-1} \text{min}^{-1}$) of adsorption, respectively. q_e and q_t are the adsorption capacity (mg g^{-1}) at equilibrium time and at time t (min), respectively. For the study of the adsorption kinetic, the initial Php concentration was 150 mg L^{-1} . The experiments were carried out using a 50 ml conical flask containing 10 ml of Php solution at pH 9.18, and the adsorbent dose was 0.0015 g mL^{-1} . Then, these samples were kept continuously stirring on a rotary shaker. At desired time intervals, the adsorbents were collected and separated by a magnet immediately for the determination of the remaining Php concentrations. The calculated values are collected in Table 8. Adsorption kinetic based on pseudo-second-order model displayed the linear plot with a correlation coefficient ($R^2 = 0.9897$). Therefore, pseudo-second-order kinetic model is appropriate for assessment of adsorption kinetic of Php on nano-composite surface.

To verify the advantage of the synthesized composites, the adsorption capacity of APM-MDAS nano-composite was compared with other previously reported adsorbents and summarized in Table 9. The results showed that the adsorption capacity of APM-MDAS nano-composite for Php was higher than that of reported related adsorbents. In addition, the adsorbent used in this work is an environmentally friendly adsorbent with the potential of industrial application. Furthermore, the magnetic property provides an easy way for particle separation.

Table 8 Kinetic model parameters for adsorption of Php on nano-composite

Pseudo-first-order model			Pseudo-second-order model		
q_e (mg g ⁻¹)	k_1 (min ⁻¹)	R ²	q_e (mg g ⁻¹)	k_2 (g mg ⁻¹ min ⁻¹)	R ²
465.372	0.053	0.697	909.091	0.004	0.989

Table 9 Comparison of adsorption capacity of APM-MDAS nano-composite with previously reported adsorbents for the adsorption of Php

Organic pollutant	Adsorbents	Adsorption capacity (mg g ⁻¹)	References
Phenolphthalein	β-CD-based polyurethanes	3.97	[32]
Phenolphthalein	Graphene/β-cyclodextrin composite	468.6	[33]
Phenolphthalein	β-CD nanomagnets	2	[34]
Phenolphthalein	Activated carbon	500.0	[35]
Phenolphthalein	PVDF@PS/PDA-24/β-CD	19.24	[36]
Phenolphthalein	β-CD/PS composite fibers	7.09	[37]
Phenolphthalein	β-CD-based polyurethanes (HDI)	19.2	[38]
Phenolphthalein	Carbon nanotubes	41.7	[35]
Phenolphthalein	APM-MDAS nano-composite	833.333	This work

Conclusion

In this work, a two-step statistical experiment design, P–B design, and CCD method were used to optimize process variables for the removal of Php from aqueous solution using APM-MDAS nano-composite. The produced nano-composite was characterized by XRD, FTIR, and SEM. By P–B screening design, three variables (initial pH, sorbent dosage, and contact time) were determined as the significant variables. The effect and interaction of the three variables were further optimized using the CCD method. After the combination of PBD and CCD, optimal removal conditions achieved were as follows: initial pH, 10.68; sorbent dosage, 0.0015 (g mL⁻¹); and contact time, 118.13 s. Under these optimal conditions, the maximum adsorption capacity of the nano-composite is found to be 833.333 mg g⁻¹, which is high. The kinetics of sorption and isotherms was discussed to analyze the adsorption mechanism and investigate the interaction between APM-MDAS nano-composite and Php. The isotherm models such as Langmuir, Freundlich, Dubinin-Radushkevich (D–R) and Temkin were applied and the data of equilibrium were finest defined by the Langmuir model. The kinetics of Php sorption fitted well with pseudo-second-order kinetic model. The results showed that the APM-MDAS nano-composite could be an effective adsorbent for Php removal and the P–B design followed by the CCD method is an effective and powerful approach for the optimization of sorption process.

Acknowledgements The authors acknowledge the financial support of this work by University of Torbat-e jam, Torbat-e jam, Iran.

References

- Z. Zhang, R.Y. Yang, Y.S. Gao, Y.F. Zhao, J.Y. Wang, L. Huang, J. Guo, T.T. Zhou, P. Lu, Z.H. Guo, Q. Wang, *Sci. Rep.* **4**, 6797–6805 (2014)
- M. Vakili, M. Rafatullah, S. Babak, A.Z. Abdullah, M.H. Ibrahim, K.B. Tan, Z. Gholami, P. Amouzgar, *Carbohydr. Polym.* **113**, 115–130 (2014)
- A. Ayati, M.N. Shahrak, B. Tanhaei, M. Sillanpaa, *Chemosphere* **160**, 30–44 (2016)
- M.N. Zafar, Q. Dar, F. Nawaz, M.N. Zafar, M. Iqbal, M.F. Nazar, *J. Mater. Res. Technol.* **8**, 713–725 (2019)
- W.H. Sun, C.J. Zhang, J. Chen, B.B. Zhang, H.Z. Zhang, Y.M. Zhang, L.J. Chen, *J. Hazard. Mater.* **324**, 739–743 (2017)
- P.V. Nidheesh, M. Zhou, M.A. Oturan, *Chemosphere* **197**, 210–227 (2018)
- Z.Z. Liu, S.J. Yang, Y.N. Yuan, J. Xu, Y.F. Zhu, J.J. Li, F. Wu, *J. Hazard. Mater.* **324**, 583–592 (2017)
- S.T. Akar, Y.Y. Balk, O. Tuna, T. Akar, *Carbohydr. Polym.* **94**, 400–408 (2013)
- V. Katheresan, J. Kansedo, S.Y. Lau, *J. Environ. Chem. Eng.* **6**, 4676–4697 (2018)
- Y. Musico, C. Santos, M. Dalida, D. Rodrigues, *J. Mater. Chem. A* **1**, 3789–3796 (2013)
- S. Ranjbari, B. Tanhaei, A. Ayati, M. Sillanpaa, *Int. J. Biol. Macromol.* **125**, 989–998 (2019)
- S.M.A.S. Keshk, A.M. Ramadan, A.G. Sehem, E. Yousef, S. Bondock, *Carbohydr. Polym.* **152**, 624–631 (2016)
- N. Jaafarzadeh, A. Takdastan, S. Jorfi, F. Ghanbari, M. Ahmadi, G. Barzegar, *J. Mol. Liq.* **256**, 462–470 (2018)

14. S. Gao, W. Zhang, H. Zhou, D. Chen, J. Rare Earths **36**, 986–993 (2018)
15. K. Hedayati, M. Goodarzi, D. Ghanbari, J Nanostruct **7**(1), 32–39 (2017)
16. F. Kavousi, M. Goodarzi, D. Ghanbari, K. Hedayati, J. Mol. Struct. **1183**, 324–330 (2019)
17. K. Hedayati, M. Goodarzi, M. Kord, Main Group Met. Chem. **39**(5–6), 183–194 (2016)
18. K.R. Reddy, K.P. Lee, A.I. Gopalan, Colloids Surf. A **320**, 49–56 (2008)
19. S. Ghattavi, A. Nezamzadeh-Ejehieh, Inter. J. Hydrogen. Energy **45**, 24636–24656 (2020)
20. R.L. Plackett, J.P. Burman, Biometrika **33**, 305–325 (1946)
21. W. Ding, P. Zhao, R. Li, Carbohydr. Polym. **83**, 802–807 (2011)
22. X.D. Xin, Q. Wei, J. Yang, L.G. Yan, R. Feng, G.D. Chen, B. Du, H. Li, Chem. Eng. J. **184**, 132–140 (2012)
23. L.H. Zhang, Q. Sun, D.H. Liu, A.H. Lu, Mater. Chem. A **1**, 9477–9483 (2013)
24. A. Norouzi, A. Nezamzadeh-Ejehieh, Phys. B **599**, 412422–412431 (2020)
25. S. Guo, D. Li, L. Zhang, J. Li, E. Wang, Biomaterials **30**, 1881–1889 (2009)
26. A. Norouzi, A. Nezamzadeh-Ejehieh, Chem. Phys. Lett. **752**, 137587–137597 (2020)
27. A.S. Guzun, M. Stroescu, S.I. Jinga, G. Voicu, A.M. Grumezescu, A.M. Holban, Mater. Sci. Eng. C. **42**, 280–288 (2014)
28. M. Nosuhi, A. Nezamzadeh-Ejehieh, Electrochim. Acta **223**, 47–62 (2017)
29. T. Tamiji, A. Nezamzadeh-Ejehieh, J. Electroanal. Chem. **829**, 95–105 (2018)
30. S. Senobari, A. Nezamzadeh-Ejehieh, J. Mol. Liq **257**, 173–183 (2018)
31. M. Nasiri-Ardali, A. Nezamzadeh-Ejehieh, Mater. Chem. Phys **240**, 122142–122156 (2020)
32. M.H. Mohamed, L.D. Wilson, J.V. Headley, K.M. Peru, J. Colloid Interface Sci. **356**, 217–226 (2011)
33. P. Tan, Y. Hu, J. Mol. Liq. **242**, 181–189 (2017)
34. R. Fuhrer, I.K. Herrmann, E.K. Athanassiou, R.N. Grass, W.J. Stark, Langmuir **27**, 1924–1929 (2011)
35. M. Vadi, V. Namavar, Orient. J. Chem. **29**, 419–425 (2013)
36. N. Gao, J. Yang, Y. Wu, J. Yue, G. Cao, A. Zhang, L. Ye, Z. Feng, React. Funct. Polym. **141**, 100–111 (2019)
37. T. Uyar, R. Havelund, Y. Nur, J. Hacaloglu, F. Besenbacher, P. Kingshott, J. Membr. Sci. **332**, 129–137 (2009)
38. M.H. Mohamed, L.D. Wilson, Nanomaterials **5**, 969–980 (2015)